Volume 15, Issue 2, 152515 (1-17)

Iranian Journal of Catalysis (IJC)

https://doi.org/10.57647/j.ijc.2025.1502.15

A quadripartite Cu_2O-CdS-$BiVO_4$-WO_3 visible-light driven photocatalyst contained three cascade Z-scheme systems: Focus on conditions' optimization, scavenging agents and the mechanism pathway towards sulfasalazine

Narges Omrani, Alireza Nezamzadeh-Ejhieh*

Department of Chemistry, Shah. C., Islamic Azad University, P.O. Box 311-86145, Shahreza, Isfahan, Islamic Republic of Iran.

***Corresponding author:** arnezamzadeh@iau.ac.ir, arnezamzadeh@iaush.ac.ir, arnezam1346@gmail.com

Original Research

Received:
14 January 2025
Revised:
14 February 2025
Accepted:
26 February 2025
Published online:
17 March 2025

© 2025 The Author(s). Published by the OICC Press under the terms of the Creative Commons Attribution License, which permits use, distribution and reproduction in any medium, provided the original work is properly cited.

Abstract:

The explosive pollution of water suppliers via the discharge of various industrial and pharmaceutical effluents prompted researchers to construct novel adsorbents and photocatalysts, especially their visible-light driven photocatalysts. A novel coupled Cu_2O-CdS-$BiVO_4$-WO_3 quadripartite nanoscale catalyst was prepared and characterized by XRD, SEM-DX, X-ray mapping, and DRS techniques. Its pHpzc was also determined to be about 9. The *Eg*-values obtained were 1.95, 1.96, 2.16, 2.38, and 2.19 for Cu_2O, $BiVO_4$, CdS, WO_3, and quadripartite catalysts, respectively. The photodegradation experiments were designed via RSM. The significance of the suggested model was confirmed by a greater model *F*-value of 26.19 than $F_{0.05,14,15} = 2.55$. The optimal run in the photodegradation of sulfasalazine (SFSZ) included the C_{SFSZ}: 7 mg/L, pH 6.25, 30 min irradiation time, 0.45 g/L of the catalyst dose, by a catalyst with a Cu_2O-CdS-$BiVO_4$-WO_3 mole ratio 3:1:1:1 under visible light illumination. The effects of the scavenging agents were also studied, and the results confirmed the critical role of superoxide in SFSZ photodegradation and the hydroxyl radicals. The photodegradation pathway obeyed the direct Z-scheme mechanism, which involved three successive binary Z-scheme components involving WO_3-$BiVO_4$, $BiVO_4$-CdS, and CdS-Cu_2O, which accumulates the photoinduced electrons in the CB-Cu_2O and the holes in the VB-WO_3, the more powerful reducing and oxidizing centers, respectively.

Keywords: Type II-heterojunction; Direct Z-scheme mechanism; Quadripartite catalyst; RSM; Antibiotics

1. Introduction

In recent decades, various synthetic pharmaceutics have critically protected humans' lives and domestic animals from many diseases. This broad use accumulates them in the environment, especially aquatic ones, causing severe environmental implications such as bacterial resistance [1–8]. Further, some pharmaceutics have high resistivity against the biodegradation, natural degradation, and phototransformation processes [9–11]. Thus, due to the continuous discharge of chemical industries and disposal from consumers into the natural environment, their accumulation in the atmosphere is increasing. Accordingly, their environmental concentration reached a few mg to g per kg in soils and water. This is high enough to yield an unhealthy environment [12].

A combined sulfa drug sulfasalazine (SFSZ) consists of sulfapyridine and salicylate via an Azo bond. It became widely used to treat rheumatoid arthritis because of its antibacterial characteristics. SFSZ has a high persistence in the environment, and thus, it was used as a pollutant model here. Due to the frequent use and discharging of personal care drugs to the environment, removing them before discharging their corresponding effluents greatly diminishes their environmental accumulation and hazards [13].

However, more physical removal techniques transfer the subjected concomitant to another phase, requiring further secondary removal [14–18]. Thus, special attention has been paid to the advanced oxidation processes (AOPs) that commonly mineralize the pollutant used in some inert/harmless species [19–23]. The best efficient AOPs' technique is the heterogeneous semiconducting materials' based photocatalysis under the semiconductor illumination process

by UV or visible photons with adequate photo energy ≥ semiconductors' band gap energy (Eg) [24–30]. The semiconductors' valence band (VB) electrons (e^-) can be excited to its conduction band (CB) under the illumination process, leaving holes (h^+) in the VB. These photoinduced e/h pairs can begin subsequent attacks on the molecules of the pollutant to degrade them [31, 32]. They also can react with the dissolved oxygen and water molecules to produce the superoxide and hydroxyl radicals, respectively, as powerful oxidizing centers to attack the pollutant used [33–36].

The major problem with efficiency in heterogeneous photodegradation is the e/h recombination; thus, when it is relatively high, the overall efficiency of the process can be drastically low [37–39]. This drawback can be overcome critically by various techniques, including converting the semiconductor to nanoscale [40–48], supporting on various supports [49–52], coupling of two or more semiconducting materials, or construction of heterojunction systems or co-catalysts [53–64], doped systems with metals/non-metals species [65–68], vacancy engineering [22, 69] etc. Thus, the coupling of nano-scale semiconductors was used to enhance the photocatalytic activity of Cu_2O, CdS, $BiVO_4$, and WO_3 in this work. In the coupled systems, charge carriers transfer between the VB and CB positions of the connected semiconductors, resulting in a critical decrease in the e/h recombination process via various mechanisms such as type(II) heterojunction, direct Z-scheme [70] and S-scheme pathways [70–73]. In the nanoscale systems, the decreased path should be traveled by that charge carriers must travel to reach the surface of the catalyst is critically decreased, resulting in a decreased e/h recombination by the elongation of electrons and holes lifetimes. Unfortunately, the difficulty in the separation of nano-scale catalysts from the suspensions has been regarded as a drawback that can be covered by their excellent advantages like high effective surface area and lower e/h recombination rate.

The p-type Cu_2O semiconductor has a small band gap of 2 eV, while the n-type CdS and $BiVO_4$, with about 2.4 eV and 2.5 eV are all visible light active photocatalysts [74]. The monoclinic $BiVO_4$ showed good photocatalytic activity in pollution removal and water splitting under simulated sunlight irradiation [74, 75]. The unique future of $BiVO_4$ is its VB constitution, which includes the coupling of the Bi 6s and O 2p orbitals. This destabilizes its electrons and acts as a driving force for upward excitation. Conversely, its coupled CB includes the V 3d, O 2p, and Bi 6p hybrid, causing a lower band. This is a significant factor in creating a direct band gap with a lower energy. Thus, despite most oxides, $BiVO_4$ can be excited under visible light illumination, resulting in a bright yellow color. Further, the coupled Bi 6s and O 2p VB orbitals improve the hole mobility, satisfying the photocatalysis process [76].

The p-type semiconductor with a direct band gap of about 2.5 eV is another visible light active photocatalyst. It is used as a sensitizer due to its absorption ability against photons of a large part of the visible region. The band edge positions of $BiVO_4$ CB and VB have been reported at 0.11 V and 2.65 V vs. NHE, while those of WO_3 at 3.3 V and 0.5 V vs. NHE, respectively. These values provide evidence of the possible formation of an n-p heterojunction between them, injecting the CB -$BiVO_4$ electrons to the CB -WO_3 to promote the e/h separation [77]. In general, in a coupled system including a large band gap semiconductor and a small band gap semiconductor with a more negative CB level, CB electrons of the small band gap material can transfer into the CB level in an extensive band gap material. Thus, this can happen between the narrow band gap $BiVO_4$ (with more negative CB) and WO_3 with a longer band gap, resulting in a higher photocatalytic activity of $BiVO_4$/WO_3 concerning the individual system [78].

We coupled Cu_2O, CdS, $BiVO_4$, and WO_3 and investigated the boosted photocatalytic activity of the obtained quadripartite photocatalyst in the photodegradation of sulfasalazine (SFSZ) in an aqueous solution. A brief characterization was done in the first part of the work [30], and the kinetics of the photodegradation and photomineralization processes were studied. Other characterization techniques were used to complete the work, and the optimal photodegradation process conditions were achieved using an experimental design optimization approach. Then, the effects of scavenging agents and the photodegradation mechanism were studied.

2. Experimental

2.1 Materials

The main chemicals used including $Cu(CH_3COO)_2.H_2O$ (> 99%), $Bi(NO_3)_3.5H_2O$ (> 99%), NH_4VO_3 (> 99%), ammonium tungstate (> 99%), NaOH (> 95%), ascorbic acid (AA: $C_6H_8O_6$) (> 99%), $CdNO_3$ (> 99%), NH_4S (> 99%), HNO_3 65%), etc., were analytical grade chemical prepared from Flucka/Aldrich Co. Sulfasalazine was prepared from Mehr Daru Co. IRAN, as a 500 mg pharmaceutical tablet. The pH of the aqueous solutions/suspensions (in distilled water) was adjusted by NaOH or HCl solution [79].

2.2 Preparations and synthesis

Each SFSZ tablet was 570.0 mg in weight, and thus, five tablets were thoroughly hand-mixed in a mortar, and 115.0 mg of the powder was added to 100 mL water. After 15 min stirring, it was filtered in a 250 mL volumetric flask and reached the mark with water. This solution was about 400 mg/L concerning SFSZ and used for diluter solutions [79].

Cu_2O NPs were obtained by dissolving 0.05 g copper acetate (0.27 mmole) in 100 mL water, followed by the addition of NaOH (0.2 g in 20 mL) under constant stirring for $Cu(OH)_2$ production. 15 mL aqueous solution of AA (0.39 g/2.2 mmole) was then added to convert Cu(II) to Cu(I) ($C_6H_8O_6$ was oxidized to $C_6H_6O_6$). At this moment, the deep blue color suspension was colorless, and a burgundy suspension was achieved, confirming Cu_2O colloid formation. It was centrifuged (> 13000 rpm), and the solid Cu_2O was water washed three times and dried at 80 °C [79, 80].

To obtain CdS NPs, 100 mL 85 mM Cd(II) solution (as the nitrate salt) was prepared and slowly added to 100 mL 100 mM ammonium sulfide aqueous solution under a stirring speed of 1200 rpm. The stirring process was then continued for another 5 h. CdS NPs product was dark yellow, separated by centrifugation, washed with water, and air dried [79–81].

A hydrothermal synthesis procedure was used to synthesize $BiVO_4$ NPs: 20 mL concentrated nitric acid (65%) was added to 20 mmole bismuth nitrate to thoroughly dissolute it (solution A). Solution B was obtained by dissolving 20 mmole NH_4VO_3 in 20 mL 0.1 M NaOH. Dissolution of each solution A or B was completed within 2 h of stirring. Then, solution A was added to B and stirred for 1 h to reach a stable homogeneous suspension. Its pH reached 7 and was transferred into a Teflon-lined stainless autoclave maintained at 180 °C for 6 h. The $BiVO_4$ NPs product (other products were N_2, NO_2, O_2, and H_2O) was separated and washed with water. The yellow $BiVO_4$ NPs were dried at 80 °C for 12 h [78, 79].

Finally, WO_3 NPs were synthesized as below. 1.07 mmole (350 mg) $H_{42}N_{10}O_{42}W_{12}$-xH_2O was dissolved in 67 mL distilled water at 80 °C under vigorous magnetic stirring. After the droplet of 45 mL concentrated nitric acid was added, it was stirred (800 rpm) at 80 °C for 70 min. This remained at room temperature for a day to settle the WO_3 precipitate. After centrifugation, WO_3 was washed with water, dried at 80 °C, and calcined at 400 °C for 70 min [79, 82].

The quadripartite Cu_2O-CdS-$BiVO_4$-WO_3 catalyst was prepared by hand-mixing the adequate weight of each component required to reach a definite mole ratio in an agate mortar for 30 min [79].

2.3 Characterizations

The samples prepared were characterized by the following techniques/instruments. A X'PertPro XRD diffractometer (Ni-filter, Cu-Kα source at 1.5406 $\AA$, Acc. Voltage: 40 kV, i: 30 mA; Netherland), An UV–Vis diffuse reflectance spectrophotometer (JASCO V 670, reference: $BaSO_4$, Japan), MIRA3LMU scanning electron microscope (TESCAN Co Czech Republic), a transmission electron Microscope Philips EM 208s (100 kV), a photoluminescence spectrophotometer (Perkin Elmer, LS 45, UK), A UV-Vis double beam spectrophotometer (UV/Vis 2100S, JASCO, power source: AC 220 V/50 Hz, quartz cells), a centrifuge instrument (Sigma, rpm: 13000, g: 15493), and a p-ion meter device (Jenway model 3505) [79].

2.4 Photodegradation experiments

A dark experiment for a 10 min string of the suspensions was done to reach the equilibrated adsorption/desorption. For a photodegradation run, 10 mL 10 mg/L SFSZ solution (pH 6.25)/0.4 g/L of the catalyst was irradiated against a 40 W W-lamp (located 10 cm above the cell). A homogeneous mass transfer during the illumination process was achieved under constant magnetic stirring. At the end of the illumination process, it was centrifuged, and the supernatant was transferred to the UV-Vis cell. The absorbance of the solution (A) at $\lambda_{max} = 359$ nm was recorded and compared to that of the blank SFSZ solution (Ao). The removed SFSZ was estimated as C/Co (corresponding to A/Ao) [79].

3. Results and discussion

3.1 Characterization studies

3.1.1 XRD patterns, morphology

The proposed quadripartite photocatalyst involves WO_3, $BiVO_4$, CdS, and Cu_2O components. This work is a continuation of previously published works where the activity of the individual, binary, and ternary systems of the four elements mentioned above was studied in the SFSZ photodegradation process. The results have been published; thus, some characterization and photodegradation results have been illustrated in detail in our published works [79, 83–88].

As mentioned above, some characterization results of the sample have been discussed in the first section of the work [79]. XRD patterns confirmed that a Cu_2O cubic (CPDS# 65-3288) [21], a CdS hexagonal phase (JCPDS# 42-1411) [89], a monoclinic $BiVO_4$ phase (JCPDS card No. 14-0688) [78], and a cubic WO_3 phase (JCPDS file no. 46-1096) [78] were formed. Substituting the pattern data in the Scherrer [90] and Williamson-Hall models [91] got the average crystallite size of 27.8 and 22.5 nm for the quadripartite catalyst, respectively.

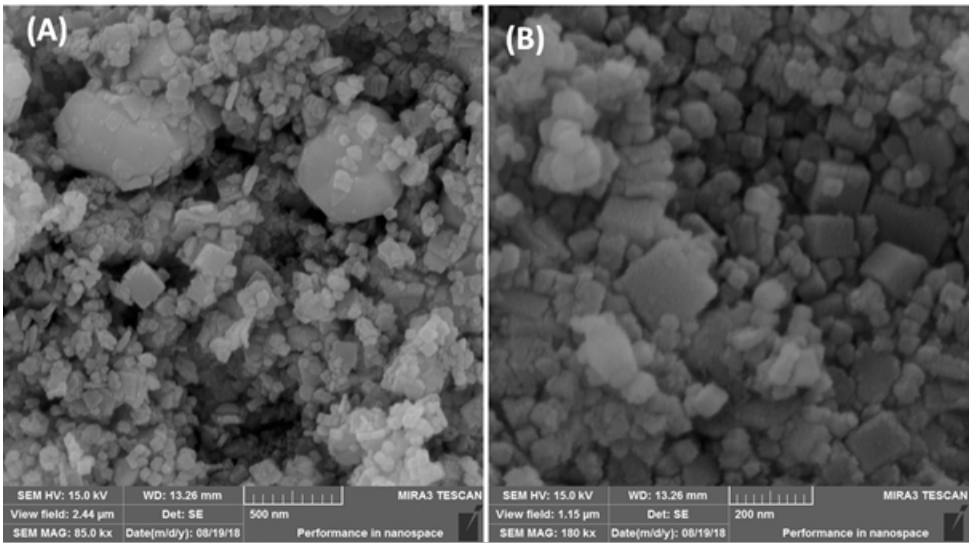

Figure 1. Some FE-SEM images of Cu_2O-CdS-$BiVO_4$-WO_3 NPs (mole ratios 3:1:1:1) [79].

The morphology of the quadripartite catalyst has also been studied, and the SEM images discussed in the previous paper [79]. Some SEM images are also presented in Fig. 1, which prove the presence of some cubes (Cu_2O and WO_3 NPs), some hexagonal relatively distorted (CdS NPs), and some nano-flakes or plate-like NPs ($BiVO_4$ species) in the catalyst. Applying the image-j software has confirmed the nano dimension for the catalyst species [79]. Elemental EXD analysis in X-ray mapping images has also confirmed the presence and homogeneous distribution of the constituent elements in the quadripartite catalyst [79].

3.1.2 Optical properties and VB/CB potential positions

Optical properties of the individual and coupled catalysts have also been evaluated by performing photoluminescence (PL) and UV-Vis spectroscopy, the results of which have been presented in the first section of the work [79]. The PL intensity was decreased in the quadripartite catalyst, confirming higher e/h separation occurred by coupling the semiconductors. Further, when the moles of the components were changed, the PL intensity changed. The sample's band gap energy (Eg) was estimated using the absorption wavelength edge obtained from the absorption spectra. The Eg-values obtained were 1.95, 1.96, 2.16, 2.38, and 2.19 for Cu_2O, $BiVO_4$, CdS, WO_3, and quadripartite catalysts, respectively [79].

Here, we use the Kubelka-Munk and the Tauc models to estimate the more precise Eg-values based on the reflectance spectra of the samples [92–96]. In the Kubelka-Munk model, the Kubelka-Munk function ($F(R) = (1 - R)^2/2R = K/S$) or the reflectance ($R$) can be converted into the absorption coefficient (α) [97] as follows. S and K are the scattering and absorption Kubelka-Munk coefficients [98].

$$K = 2\alpha = SF(R)$$

The Eg value for various electronic transitions can be estimated from the following Tauc relation:

$$F(R)h\upsilon = A(h\upsilon - Eg)^n$$

Depending on the type of transition that occurs, the power n gets various values. Depending on the electronic nature, the exponent n-value gets values of 3, 2, 3/2, and 1/2 for the indirect forbidden (IF), indirect allowed (IA), direct forbidden (DF), and direct allowed (DA) transitions, respectively [99]. By the change in writing format for this equation, the n-value tends to change. For example, an n value equal to 1/2 for a direct band gap material is subjected to the above-mentioned formula. This equation can be rewritten for this direct electronic transition, and an n value of 2 must be achieved. In the following formula, an n value of 2 is for a DA transition, a value of 1/2 is for an IA transition, a value of 2/3 is for a DF transition, and a value of 1/3 is for an IF transition [100].

$$(F(R)h\upsilon)^n = A(h\upsilon - Eg)$$

Due to s-d and p-d exchange interactions, a red shift in the band gap energies has been reported [101].

In the following format, n values of 1/2, 3/2, 2, and 3 show the DA, DF, IA, and IF transition, respectively [102–104].

$$(\alpha h\upsilon)^{1/n} = A(h\upsilon - Eg)$$

We can write the following model: the exponent $n = 2$ is for DA transition, $n = 2/3$ for DF transition, $n = 1/2$ for IA transition, and $n = 1/3$ for IF transition [105, 106].

$$(\alpha h\upsilon) = A(h\upsilon - Eg)^{1/n}$$

If the equation is written as follows, n gets values of 1, and 4, for DA and IA transitions, while the values of 3 and 6 for DF and IF transitions, respectively [107].

$$(\alpha h\upsilon) = A(h\upsilon – Eg)^{n/2}$$

This formula can construct a plot of ln ($\alpha\ h\upsilon$) vs. ln ($h\upsilon - Eg$) with an approximate Eg-value. The slope of a straight line gives the value of n for the transition investigated. For calculating the Eg-value, a plot of $(\alpha h\upsilon)^{2/n}$ vs. $h\upsilon$ should be constructed, providing a tangential line. This line is near the band edge. The extrapolation of the rising slope of the curve towards the x-axis of the photon energy, the obtained x-intercept is equal to the optical band gap [107].

Finally, in another format of the Kubelka-Munk equation, n values of

$$(\alpha h\upsilon)^{2/n} = A(h\upsilon – Eg)$$

Based on the reflectance data (Fig. 2 (A)), the Tauc plots were constructed as shown in Fig. 2 (B) and SDF1 (supplementary data). As shown in Fig. 2 (B), WO_3 NPs showed the most significant Eg, which can be lowered effectively when coupled with other semiconductors. The results obtained are summarized in Table 1, confirming that the as-synthesized catalysts are visible light active. The band gap energies for $BiVO_4$ and WO_3 NPs synthesized here showed a blue shift concerning the commercial $BiVO_4$ ($Eg = 2.3$ eV) and commercial WO_3 ($Eg = 2.6$ eV) due to the increased Eg in nanoscale [76].

In the next step, the catalyst's VB and CB potential positions were calculated by the following formulas: the free electrons energy is about 4.5 eV (vs NHE), and χ is the semiconductor's electronegativity [110]. This calculation illustrated the reasons for the increased separation rate of the photoinduced e/h pairs.

$$E_{CB} = \chi - E^e - 1/2Eg$$

$$E_{VB} = E_{CB} + Eg$$

The χ value of each semiconductor is a geometric mean of the electronegativity of each constituent element. As shown in Table 1, the atoms' electronegativity can be estimated from the atom's first ionization and electronegativity energies.

3.1.3 pHpzc

Exposing some metal oxides to the external environment, especially aqueous ones, changes the surface characteristics and significantly changes the accumulated surface charge. This is based on the proton balance between the solid surface and the aqueous suspension prepared, and the equilibrium adsorption/desorption reached would be expected to

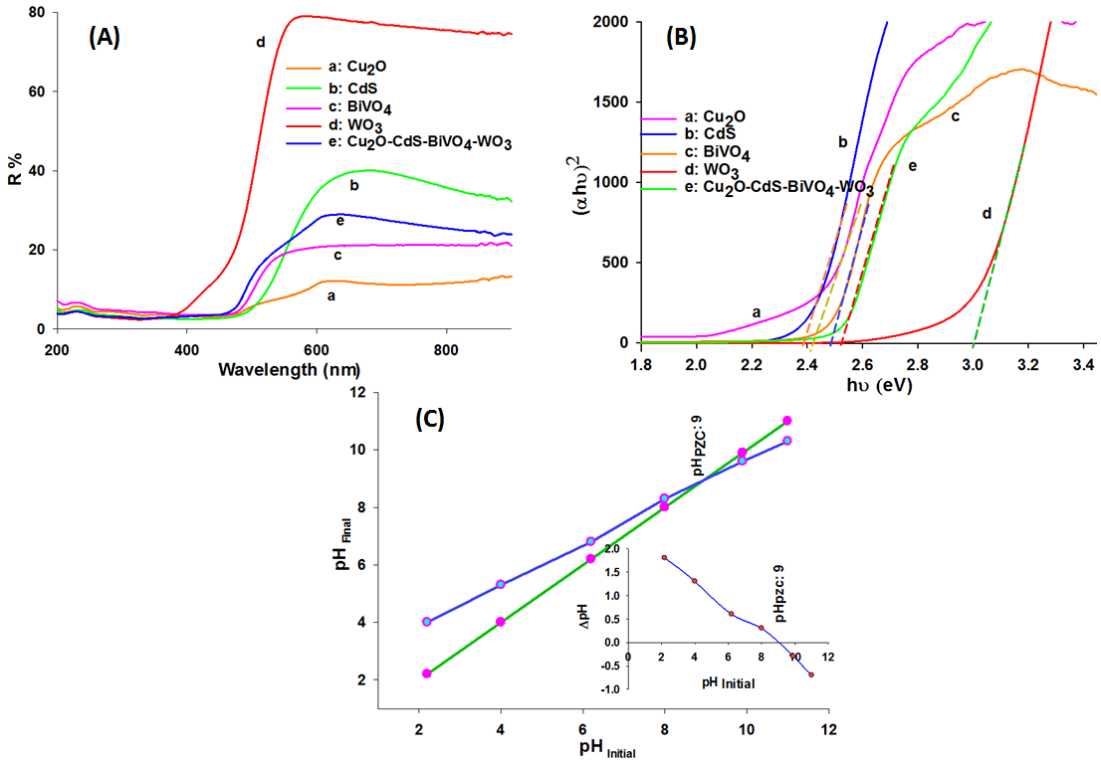

Figure 2. (A) Typical UV–Vis reflectance spectra obtained in DRS study of the Cu_2O, CdS, $BiVO_4$, WO_3 NPs and Cu_2O-CdS-$BiVO_4$-WO_3 quadripartite sample (mole ratios 3:1:1:1); (B) Typical Tauc plot for $n = 2$ obtained based on reflectance spectra in case A; (C) Typical plots for calculation of pHpzc of Cu_2O-CdS–$BiVO_4$-WO_3 [79].

be forced by their acid-base futures. Commonly, the surface hydroxyl groups of the metal oxide can alter the surface electrical charges in an aqueous environment [42, 111]. In general, the electrolyte concentration, pH, and the native properties of the solid material used can change the type of accumulated charges on the surface. This pH dependency of the surface charge of mineral adsorbents/catalysts in an aqueous phase is critical in the overall process yield. Thus, to obtain more reliable optimal conditions for running the process, it is essential to know about the accumulated surface charge [112].

A critical pH point for describing the surface accumulated charge is the zero charge (pHpzc or PZC), in which the surrounding solution neutralizes the surface accrued charge. An equal number of de-protonated negative surface centers must balance the positive surface centers (via the protonation process). In general, knowing the pHpzc point of the sample used is very important, and it has been reported that the chemical properties of some soil samples and mineral oxides or hydroxides can be determined by their pHpzc future. The PZC characteristics played a critical role in the overall efficiency of some processes, such as ore flotation, adsorption of colloidal particles on the surface, etc. Further, the deposition efficiency of the corrosion products in steam generators and the transporting radioactivity efficiency in a water-cooled nuclear reactor can be illustrated by the pHpzc of the surface subjected [112].

Typical plots for determining the pHpzc of the quadripartite catalyst are shown in Fig. 2. Before the pHpzc, the native basic or negative surface could adsorb protons from the adjacent aqueous phase, resulting in net positive surface charges and increase in the suspension pH (please focus on Fig. 2). Beyond the pHpzc, the native acidic or positive future of the surface adsorbs hydroxyl anions from the adjacent aqueous media, resulting in a net negatively surface charge and a decreased suspension pH. The quadripartite catalyst showed a pHpzc around 9.

3.2 Photocatalytic studies

3.2.1 The boosted photocatalytic activity of the coupled system

Some preliminary removal runs were done to evaluate the capability of the quadripartite catalyst in SFSZ removal; the results have been discussed in the first section of the work [79]. The results are also shown in Fig. 3. Briefly, a dark experiment for 10 min was done to achieve an equilibrated surface adsorption/desorption process [113] based on the preliminary experiments illustrated in the first part of the work. Then, the photodegraded solutions were compared against the direct photolyzed solution to obtain a net photodegradation efficiency. Based on the decrease in the peak intensity of the photodegraded solutions, the photodegradation efficiencies of 6, 27, 39, and 48% were achieved for $BiVO_4$, WO_3, CdS, and Cu_2O NPs in SFSZ photodegradation when used alone. This efficiency was enhanced to about 64% when the coupled quadripartite catalyst was used. This boosted effect is related to the faster separation of the photoinduced e/h pairs, which will be discussed in detail in the following sections by constructing suitable schematics. Based on the results [79], the change in the mass ratio of the components of the quadripartite catalyst, changed the PL

intensity and the photodegradation efficiency. The lowest PL intensity and the highest photocatalytic activity were obtained when the quadripartite catalyst with a Cu_2O:CdS:$BiVO_4$:WO_3 mole ratio of 3:1:1:1 was used. In general, both the higher extent of the production of the e/h pairs and their lower recombination extent determine the overall efficiency of the process. These can be changed by varying the semiconductor components in the catalyst, reaching the optimal extents in the above-mentioned ratio [114]. Thus, this catalyst was used in the experimental design optimization approach to optimize the SFSZ photodegradation condition. The results will be discussed in the next section.

3.2.2 Experimental design (RSM) studies

Table 2 summarizes the selected influencing variable in the RSM study of SFSZ photodegradation process. The selected

Table 1. Band gap and potential positions for CB and VB of the semiconductors used.

Approximated band gap energies of the used catalysts by using the absorption edge method and Kubelka-Munk equation and Tauc plots						
Catalysts	**Tauc plots (eV)**				**Absorption edge**	
	1/2	2	3/2	3	λ (nm)	Eg (eV)
Cu_2O	2.665	2.412	2.445	2.425	636	1.949
CdS	2.667	2.382	2.489	2.487	573	2.164
$BiVO_4$	2.389	2.43	2.508	2.519	566	2.190
WO_3	2.820	2.998	3.011	3.027	634	1.955
Composite	2.453	2.523	2.549	2.562	520	2.384

E_a and E_i values of the constituent elements of the used semiconductors			
Element	E_a (eV)	E_i (eV)	$1/2(E_a + E_i)$ (eV)
Cu	1.235	7.712	4.475
O	1.461	13.618	7.539
Cd	0.724	8.985	4.854
S	2.077	10.358	6.217
Bi	0.942	7.238	4.090
V	0.527	6.739	3.633
W	0.816	7.864	4.340

Eg, V_B and C_B values of the used semiconductors, χ data are in Mulliken's electronegativity scale				
Catalyst	χ (eV)	Eg (eV)	E_{VB} (eV)	E_{CB} (eV)
Cu_2O	5.35	2.41	2.05	-0.36
CdS	5.49	2.38	2.18	-0.20
$BiVO_4$	6.02	2.43	2.73	0.30
WO_3	6.56	2.99	3.55	0.56

Various formats for the Tauc model					
	***n*-value for:**				
Formula	IF	IA	DF	DA	Ref.
$F(R)h\upsilon = A(h\upsilon - Eg)^n$	3	2	3/2	1/2	[99]
$(F(R)h\upsilon)^n = A(h\upsilon - Eg)$	1/3	1/2	2/3	2	[101]
$(\alpha h\upsilon)^{1/n} = A(h\upsilon - Eg)$	3	2	3/2	1/3	[103, 108, 109]
$(\alpha h\upsilon) = A(h\upsilon - Eg)^{1/n}$	1/3	1/2	2/3	2	[105, 106]
$(\alpha h\upsilon) = A(h\upsilon - Eg)^{n/2}$	6	4	3	1	[107]
$(\alpha h\upsilon)^{2/n} = A(h\upsilon - Eg)$	6	4	3	1	[107]

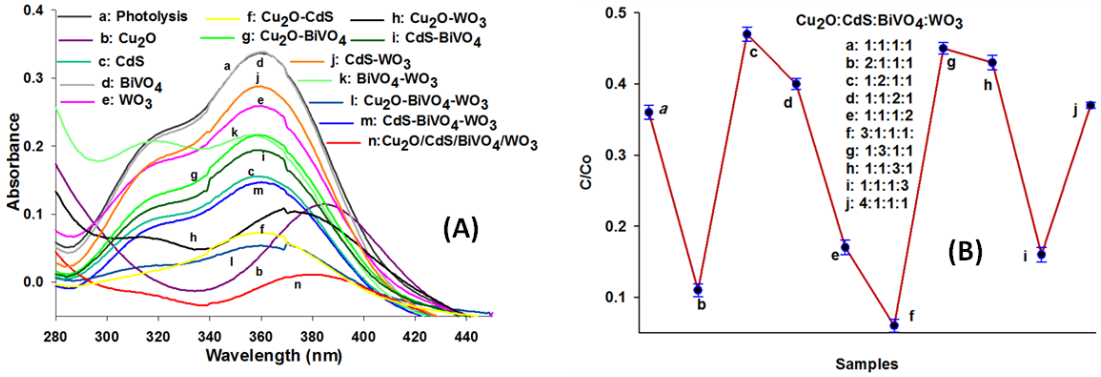

Figure 3. (A) Effects of direct photolysis and photocatalytic processes on SFSZ removal (catalysts dose 0.4 g/L, C_{SFSZ}: 10 mg/L, irradiation time: 30 min, initial pH 6.5); (B) Effects of the mole ratio of the Cu_2O:CdS:$BiVO_4$:WO_3 in photodegradation of SFSZ [79].

ranges include the axial level (±2), the cubic level from the factorial design (±1), and the central level (with a code of 0). Based on the selected ranges for each variable, a central composite design (CCD) was constructed by inputting the ranges to the software, which resulted in the suggestion of conditions for 30 runs (16 factorial (2^4), 8 axial (2k, k = number of factors), and 6 center point replicates). The coded values were obtained by the following formula: the coded and actual values of the independent variable (X_i and X_j) are X_{ci} and X_i, while its actual value at the center point is Xo. ΔX is the value of the step change [115].

$$x_{ci} = \frac{(Xi - Xo)}{\Delta X} \quad (1)$$

After performing the photodegradation experiments based on the RSM runs' conditions, the viable response Y (SFSZ photodegradation%) was inputted into the software. The coefficients (β_0: the constant intercept, β_i, β_{ii}, and β_{ij}: the linear, second order, and interactive effects regression coefficients, respectively) of the following quadratic (second order) were determined as shown in equation (2) [115, 116].

$$Y = \beta_0 + \Sigma\beta_i x_i + \varepsilon = \beta_0 + \Sigma\beta_i x_i + \Sigma\beta_{ii} x_i^2 + \Sigma\beta_{ij} x_i x_j + \varepsilon \quad (2)$$

$$Y(\text{Deg.}\%) = 28.68 - 3.82A - 11.83B + 13.57C + 0.43D - 3.33AB - 2.92AC + 0.81AD - 5.24BC + 3.32BD + 12.20CD - 0.51A^2 + 8.99B^2 + 3.79C^2 - 2.55D^2 \quad (3)$$

3.2.3 Anova and Fit summary

Other data in Table 2 belong to the ANOVA (analysis of the variance) analysis constructed based on the Fischer test (F-test) analysis. The significance of the model suggested can be evaluated by comparison of the model F-value of 26.19 (a divide of model MS to that of residual) with the critical value of $F_{0.05,\ 14,\ 15} = 2.55$. This larger calculated F-value confirms that the suggested model can significantly process more than 95% of the data obtained, and only less than 5% cannot be processed. The model lack of fit (LOF) estimates the random errors, and for a significant model, this term must be not significant. Here, the LOF F-value (a divide of its MS to that of pure error) is 2.04, smaller than the tabulated $F_{0.05,\ 10,\ \text{and}\ 5} = 8.79$. This smaller calculated F-value confirms a non-significant LOF, proving that random errors influenced the data obtained [117, 118].

The correlation coefficients, including the multiple correlation coefficients R^2 ($R^2 = 0.9607$), adjusted-R^2 (adj-$R^2 = 0.9240$) and predicted-R^2 (pred-$R^2 = 0.8070$) were achieved. All values are close to unity, confirming a reasonable statistical data fit in the model [119].

A precision measure of the model can be evaluated by the CV (coefficient of variation) term, and a smaller CV value shows higher model precision. Here, a CV value of 7.20% was obtained, which is relatively low. Further, an adequate precision value of 19.80 was achieved, and in RSM, this value must be above 4 for a good model. This term estimates the S/N ratio in the space investigated or to navigate the design space [120].

3.2.4 Diagnostic plots

Diagnostic plots are shown in Fig. 3 (A) and SDF2. The normal probability plot in Fig. 3 (A) confirms normal distribution of residual around the normal diagonal straight line with no trend. No transformation is required because no S-shaped curve was reached. The plot of residuals versus predicted response values tests the assumption of constant variance across the graph, which is confirmed by a random scatter.

As shown here, a typical plot of residuals versus an experimental run should show a random scatter to check the lurking variables that may influence the response variable during the experiment. The plot of actual responses versus the predicted responses detects a value or group of values the suggested model does not predict. This can be confirmed by a split of data points evenly by the 45-degree line.

3.2.5 Influencing plots

The influencing plots show the influence of individual runs, which are shown in Fig. 3 (B) and SDF3. Based on the externally studentized residual (outlier t, R-student) no outlier point is present because no data point is laid out of the control limits ±3. The outlier data points are not fitted well by the proposed model, due to a wrong value or model. The applicability of a definite data point to influence the model fit can be evaluated by the leverage-run plot, in which each run gets a numerical value between zero and one. A high leverage value near one proves the predicted and actual val-

ues have the same force with zero residual, which is terrible because an unexpected error source influenced the model. The difference in fit can be evaluated by plotting DFFITS versus runs, and the value can be estimated by deleting the point and following the change in the fit. Thus, a larger DFFITS value proves more influence on the point in the fitted model. Mathematically, this is similar to the externally studentized residual with a high leverage point. The plot of Cook's distance versus runs measures the change in the regression when the case is deleted. Large values ($2-3$ times

Table 2. Data used/obtained in the RSM study of SFSZ removal by the quadripartite Cu_2O-CdS-$BiVO_4$-WO_3 catalyst.

Variables and surfaces for the design of experiment by RSM under CCD pattern					
Code/Factor	Unite	-1 level	+1 level	-α	+α
X1: **Contact time**	min	20	40	10	50
X2: **Ads. dosage**	mg/L	0.3	0.6	0.15	0.75
X3: C_{SFSZ}	mg/L	8	10	7	11
X4: pH	-	3.5	9	0.75	11.75

Analysis of variance (ANOVA) for *%degradation* of SFSZ					
Source	Sum Sq.	df	Mean Sq.	F value	p-value
Model	14412.82	14	1029.49	26.19	<0.0001 **Sig.**
X1: time	4417.58	1	4417.58	112.36	<0.0001
X2: Ads. Dos.	4.39	1	4.39	0.11	0.0074
X3: $C_{pb(II)}$	3359.96	1	3359.96	85.46	<0.0001
X4: pH	22.44	1	22.44	3.31	0.0089
X1X2	2380.22	1	2380.22	60.54	<0.0001
X1X3	438.59	1	438.59	11.16	0.0045
X1X4	136.71	1	136.71	3.48	0.0082
X2X3	175.89	1	175.89	4.47	0.0052
X2X4	10.61	1	10.61	0.27	0.0061
X3X4	176.96	1	176.96	4.5	0.0509
$X1^2$	394.18	1	394.18	10.03	0.0064
$X2^2$	178.22	1	178.22	4.53	0.0502
$X3^2$	2218.48	1	2218.48	56.43	<0.0001
$X4^2$	7.25	1	7.25	0.18	0.6738
Residual	589.72	15	39.31		
Lack of Fit	473.66	10	47.37	2.04	0.2231 **not sig.**
Pure Error	116.06	5	23.21		
Cor Total	15002.54	29			

The results obtained for the applicability of the model	
Variable	Value/Type
Optimized values	pH: 9, Dose: 0.45 g/L, time: 30 min, C_{SFSZ}: 6.25 mg/L
Suggested model	Quadratic
Predicted response	90.70
95% CI low and high	86.6-95.0
Predicted Std Dev	2.3
Observed response (n=3)	95 ± 2.3

greater than the other points) commonly have high leverage and large studentized residuals; thus, these values must be re-investigated. Finally, all diagnostic and influencing plots confirmed the goodness of the model suggested (Fig. 4).

3.2.6 Model graph

3D and related 2D contour plots are summarized in Fig. 5 and SDF3 to present the simultaneous interactions between the binary variables investigated graphically. The suspension pH is a crucial experimental variable that critically influences the response. It simultaneously affects the accumulated charges on the catalyst's surface and the SFSZ molecules' ionic species. Depending on the pKa values of 2.4, 6.8, and 11 that have been reported for SFSZ salicylic ring, ulphonamide hydrogen, and azo bond or pyridine rings' nitrogen atoms, respectively [115], SFSZ molecules can be present as various ionic species depending the pH of the suspension.

Thus, it would be expected that at acidic pHs around 3.5, the ulphonamide hydrogen and the nitrogen atom of the azo bond or pyridine ring to be in the protonated form should be repelled by the positively charged surface of the catalyst (see pHpzc section). This negative effect can continue at pHs about 9, because the mentioned nitrogen atoms may be in the protonated form.

The concentration of the pollutant can change the collision probability between SFSZ molecules and the catalyst surface, where the reactive species with very short lifetimes are formed and absorb the arrived photons by the catalyst surface. Due to the lower collision probability at low concentrations, the reactive species may participate in the side reaction, resulting in photodegradation efficiency. The increased collision probability due to the increased concentration can increase the photodegradation efficiency. However, high amounts of the arrived photons may be absorbed in the high SFSZ concentration, adversely affecting the photodegradation of SFSZ molecules. Thus, an optimal concentration value would be expected. Thus, in Fig. 5 (A), through the pH range of $3.5-9$, the photodegradation efficiency cannot be increased at high concentrations, and the best optimal interactions between pH-C can be achieved at moderate concentrations of 8 ppm. Based on the results in Fig. 5 (B), the negative effects of the pH range of $3.5-9$ cannot be compensated by shorter irradiation times.

The catalyst dose can affect both the aggregation of the solid powder and the amounts of active centers to be illuminated. With mass increasing the catalyst, more active centers can be illuminated to produce the reactive species. At the same time, it aggregates the catalyst species and reduces the effective surface area under illumination. As shown in Fig. 5 (C), a moderate dose of 0.45 g/L at more acidic pHs caused a better photodegradation efficiency. In this pH, the ulphonamide hydrogen may be released, and thus, an attractive force between this segment and the catalyst surface may attract SFSZ molecules and bring them near the surface to be degraded.

The interactions of C-Time in Fig. 5 (D) confirm that moderate concentrations of 8 ppm have better collision probability than 10 ppm, resulting in a more extended degradation yield. This confirms that some resist intermediates may form, needing longer illumination times to be degraded. The adverse effects of higher doses of the catalyst can be compensated by using relatively lower concentrations (Fig. 5 (E)) and longer irradiation times (Fig. 5 (F)).

The model's applicability was evaluated by performing SFSZ photodegradation runs in the optimal runs' conditions of pH 6.25, catalyst dosage 0.45 g/L, irradiation time 30 min, C_{SFSZ}: 7 g/L. The results were averaged based on triplicate measurements and compared with the acceptable range suggested by the model. Good agreement between them confirms the applicability of the proposed model in SFSZ photodegradation (Table 2).

3.2.7 Scavenging agent's effects and the photodegradation mechanism

As illustrated in the introduction section, in a typical heterogeneous photocatalytic process, the main reactive species of e^-, $^\bullet O_2^-$, h^+, and $^\bullet OH$ produced under the appropriate light irradiation are responsible for the degradation of various organic pollutants. To estimate their relative importance in the degradation reaction, the change in the photodegradation activity of the proposed quadripartite catalyst in the presence of $K_2S_2O_8$, $KHCO_3$, acetic acid, and ascorbic acid (AA) as the scavenging agents were followed. The proposed trapping agents can respectively trap the photoinduced electrons (e^-), hydroxyl radicals ($^\bullet OH$), photoinduced holes (h^+), and superoxide ion radicals ($^\bullet O_2^-$), respectively. Accordingly, the scavenging of each reactive species must

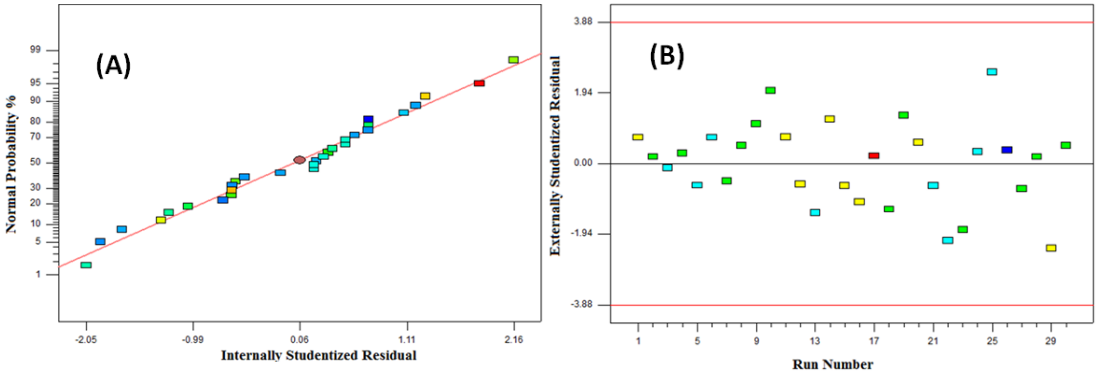

Figure 4. Typical diagnostic (A) and influencing, (B) plots obtained in RSM study of SFSZ by Cu_2O-CdS-$BiVO_4$-WO_3 catalyst.

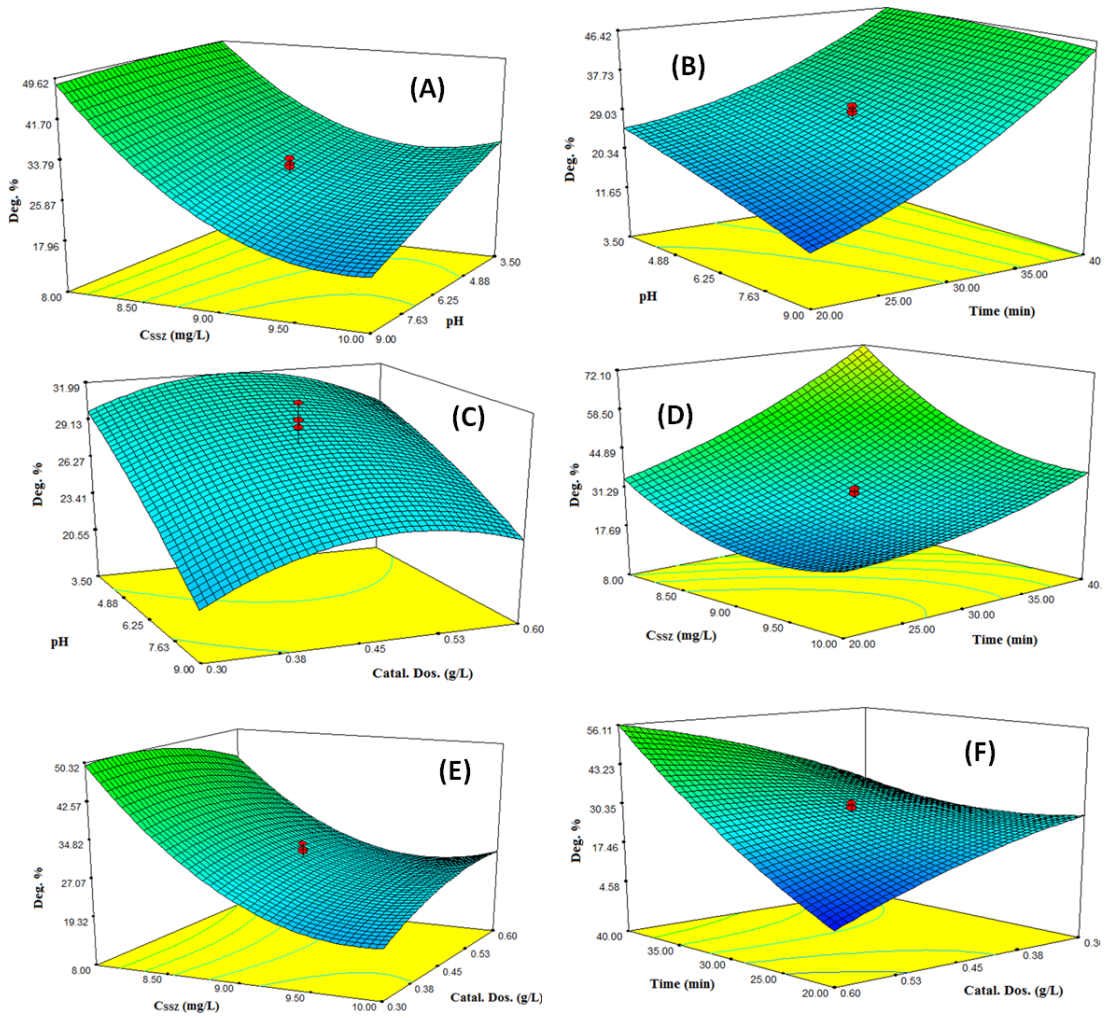

Figure 5. 3D response surface plots for effects of process variables on SFSZ by Cu_2O-CdS-$BiVO_4$-WO_3 catalyst.

decrease overall photodegradation efficiency, proving the higher role of the investigated reactive species in the photodegradation process. The photodegradation results are shown in Fig. 6 (A). Peroxodisulfate (PDS), peromonosulfate and hydrogen peroxide, are known as electron scavengers in the heterogeneous photocatalytic process. During this scavenging process, PDS production is sulfate anion radicals ($SO_4^{\bullet-}$). Following rate constants have been reported for PDS and sulfate radicals contained reactions in acidic pH range of $3-8$ [121].

$S_2O_8^{2-} + \text{Heat} \rightarrow 2SO_4^{\bullet-}$

(k_1: 5.7×10^{-5} s^{-1})

$SO_4^{\bullet-} + S_2O_8^{2-} \rightarrow S_2O_8^{\bullet-} + SO_4^{2-}$

(k_2: 6.1×10^{-5} $M^{-1}s^{-1}$)

$SO_4^{\bullet-} + H_2O \rightarrow {}^{\bullet}OH + H^+ + SO_4^{2-}$

($k_3[H_2O] < 2 \times 10^{-3}$ $M^{-1}s^{-1}$)

$SO_4^{\bullet-} + SO_4^{\bullet-} \rightarrow S_2O_8^{2-}$

(k_4: 5×10^8 $M^{-1}s^{-1}$)

The powerful ($^{\bullet}OH$) for photochemical decontamination in freshwater can be photochemically generated by illuminating nitrate, nitrite, and dissolved organic matter (DOM). Simultaneously, many solutes, such as DOM itself, can scavenge these radicals and inorganic carbon as carbonate and bicarbonate salts. The scavenging reaction kinetics of $^{\bullet}OH$ and carbonate or bicarbonate obey a second-order model with rate constants of $3.9 \div 10^8$ M^{-1} s^{-1} and 8.5×10^6 M^{-1} s^{-1}, respectively. The produced $CO_3^{\bullet-}$ is less reactive than $^{\bullet}OH$ [122].

Acetic acid is known as an effective hole scavenger [123]. Ascorbic acid undergoes the one or two electron steps redox reactions that form semidehydroascorbic acid and dehydroascorbic acid ($DHA + 2H^+ + 2e^- \rightarrow ASC + H_2O$, E^o (pH 7) = 60 mV) [124]. AA is a superoxide radical scavenger, and in the presence of acetaldehyde and xanthine oxidase (as the superoxide radical sources), the second order rate constant of 8.2×10^7 $M^{-1}s^{-1}$ has been reported for the scavenging of superoxide by AA. Another first-rate constant for such scavenging reaction has been reported as 2.7×10^5 $M^{-1}s^{-1}$ (in the presence of a xanthinexanthine oxidase system) [125].

As depicted in Fig. 6 (A), the inhibition trend is ascorbic acid > acetic acid > $KHCO_3$ > $K_2S_2O_8$, proving that the critical photodegradation role by the proposed catalyst belongs to the photogenerated $^{\bullet}O_2^-$ and then to $^{\bullet}OH$. The results show that the photoinduced e^- and h^+ species play a minor role during the photodegradation reaction. Based on the results obtained here and using the VB/CB potential positions obtained in DRS section, the photodegradation mechanisms were proposed, which will be discussed in the following.

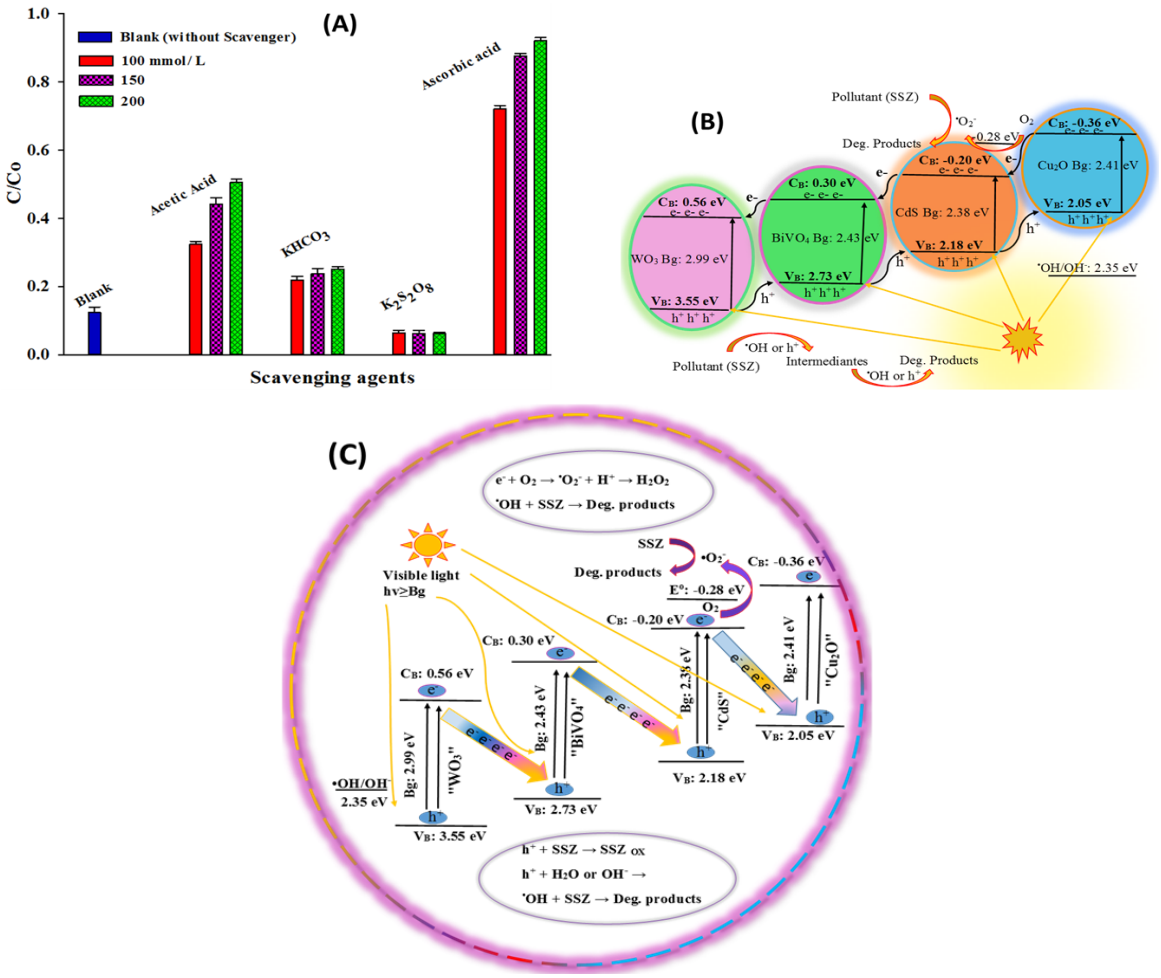

Figure 6. (A) Effects of some scavenging agents in SFSZ photodegradation (catalysts dose g/L, C_{SFSZ}: mg/L, irradiation time: min, initial pH); (B-C) Proposed mechanism for SFSZ photodegradation by the proposed Cu_2O-CdS-$BiVO_4$-WO_3 photocatalysts.

So far, various mechanisms have been described to illustrate the photodegradation pathways in heterogeneous photocatalysis. These mechanisms involve direct Z-scheme photocatalysts, traditional Z-scheme photocatalysts, all-solid-state Z-scheme photocatalysts, type II-heterojunction systems, etc. [126–128].

In heterojunction systems, the Type-II photocatalytic mechanism is usually the most common. This mechanism is shown in Fig. 6 (B) when the coupled semiconductors are considered successive binary heterojunction systems. Under the visible light irradiation of the system, all components can be excited to produce the e/h pairs. Among the CB positions, the CB-Cu_2O has a more negative (higher) potential position (−0.36 V) than that of CB-CdS (−0.28 V), satisfying the electron transfer from CB-Cu_2O to CB-CdS direction. Consequently, the CB-CdS electrons can rapidly transfer to that of the CB-$BiVO_4$ position with a more positive potential position (0.3 V). The final goal of these electrons is the CB-WO_3 position with the most possible position (0.36 V) among all CB positions involved.

Meanwhile, the photogenerated holes' transfer obeys a reverse path from the VB-WO_3 (3.55 V) to VB-$BiVO_4$ (2.73 V), then to VB-CdS (2.73 V) and finally to VB-Cu_2O (2.05 V). Overall, these e/h migrations result in the accumulation of the photogenerated electrons in the CB-WO_3 (0.56 V) and the holes in the VB-Cu_2O (2.05 V). These successive reduction/oxidation steps between the coupled components promote the spatial separation of the photoinduced e/h pairs, resulting in a suppressed recombination for the photoinduced e/h charge carriers. Overall, this quadripartite catalyst can be considered as three type-II-heterojunction component involving the WO_3-$BiVO_4$, $BiVO_4$-CdS, and CdS-Cu_2O. On the other hand, this system can be regarded as a typical cascade type(II) heterojunction system in which the above mentioned binary type(II) heterojunction systems are consequently connected.

This suggested type(II) heterojunction system is not capable of producing sufficient superoxide radicals because the accumulated CB-WO_3 electrons with a very positive potential position (E: 0.56 V) concerning that of oxygen reduction (E: −0.28 V) cannot reduce the dissolved oxygen to superoxide radicals. In this suggested mechanism, only superoxide radicals can be produced by the electrons in the CB-Cu_2O, which is relatively free from the photogenerated electrons due to the successive migrations towards CB-WO_3. Similarly, the difference in the potential positions of the photoaccumulated hole in the VB-Cu_2O (E: 2.05 V) and that of water oxidation to produce hydroxyl radicals (E: 2.35 V) is tiny to the effective production of enough hydroxyl radicals. This proposed successive type

II-heterojunction charge transfer pathway for the proposed quadripartite catalyst is unsuitable for producing enough superoxide and hydroxyl radicals under the illumination process. Furthermore, if direct degradation of SFSZ molecules by the photoinduced electrons is considered a type of SFSZ degradation, its efficiency is also low. The direct oxidation potential of SFSZ molecules has been reported to be about 0.75 V [129], and its difference with that of CB-WO_3 is about 0.2 V. Thus, SFSZ cannot be degraded effectively (reduced) by the photoaccumulated CB-WO_3 electrons.

Thus, we considered another charge carrier transfer pathway to illustrate the excellent SFSZ degradation efficiency obtained by the proposed photocatalyst based on the results obtained in the study of scavenging agents. The direct Z-scheme photocatalysts are patterns like natural photosynthesis systems with outstanding merits of high light harvesting, critical spatially separated reductive and oxidative active centers, and a well-preserved powerful redox characteristic. Thus, such a system has been widely used in photocatalysis, photodegradation, water splitting for O_2 and H_2 evolution, photoreduction of CO_2 to produce hydrocarbon fuels, etc [130–135]. According to the direct Z-Scheme mechanism, the typical schematic is presented in Fig. 6 (C), which consists of 3 binary Z-scheme systems, including the WO_3-$BiVO_4$, $BiVO_4$-CdS, and CdS-Cu_2O, which are sequentially connected. On the other hand, this system can be considered a typical cascade direct Z-scheme system in which the binary direct Z-schemes mentioned above are consequently connected.

The first Z-scheme system involves WO_3-$BiVO_4$, in which the potential positions of CB-WO_3 (0.56 V) are negative enough to transfer its photoinduced electrons to the VB-$BiVO_4$ (2.73 V), which can be photoexcited to CB-$BiVO_4$ position (0.3 V). The second Z-scheme system can then form, and the VB-$BiVO_4$ photoinduced electrons (0.3 V) can transfer to the VB-CdS position (2.18 V), which can be photoexcited to its CB position (−0.28 V) to form the $BiVO_4$-CdS Z-scheme system. The electron transfer from the Cb-CdS (−0.28 V) to VB-Cu_2O (0.2.05 V) and the final photoexcitation to the CB-Cu_2O (−0.36 V) construct the third Z-scheme component. On the other hand, based on the migration of the CB-CdS electrons to the VB-Cu_2O position, the final path of the photoinduced electrons is CB-Cu_2O. These CB-Cu_2O accumulated electrons are more powerful reducing centers (−0.36 V) than the CB-WO3 accumulated electrons in type II-heterojunction mechanism in the CB-WO_3 position (0.56 V), and capable of producing enough superoxide radicals via the reduction of high amounts of the dissolved oxygen. These electrons can also directly reduce SFSZ molecules (E: about 0.75 V). As proved by scavenging agents, superoxide radicals can also react with SFSZ molecules, which is the more effective species in its degradation. In this direct Z-scheme mechanism, the holes must be accumulated in VB-WO_3 (3.55 V), which are more powerful oxidizing agents than those collected in the VB-Cu_2O (2.05 V) in the type II-heterojunction system. These accumulated holes can effectively oxidize water to hydroxyl radicals, as the second critical active centers for SFSZ photodegradation based on the results obtained in the scavenging agent study. Based on the results, the successive direct Z-scheme system is suitable for illustrating the SFSZ photodegradation using the proposed quadripartite catalyst.

3.2.8 Reusability of the catalyst

The reusability of the fabricated photocatalyst was kinetically evaluated as a critical economic issue, and the results obtained were illustrated in detail in the first part of the work [79]. After the photodegradation of SFSZ under optimized RSM runs' condition, but under various illumination times, the reused catalyst was washed and dried at 100 °C for 20 min for the next run. Three reusing runs were performed, and the average value was obtained each time based on triplicates. Based on the results, typical Hinshelwood plots were constructed, and average slopes of 0.065 ± 0.010, 0.053 ± 0.007, and 0.054 ± 0.004 min^{-1} were calculated for the first to third runs, respectively, as the pseudo-first order rate constant, k. To validate the reusability of the catalyst statistically, the statistical 't-test' approach was used based on the pooled standard deviation of 0.008 min^{-1} obtained in three classes of data runs. The smaller calculated t-value of 1.77 than the critical value of $t_{0.05,\,4} = 2.78$ [76], proved that there is no considerable difference between the k-values obtained. Thus, the activity of the photocatalyst critically remained after 3 reusing runs at the considered time interval [79]. It is worth mentioning that individual CdS photocatalysts suffer from the photo corrosion effect. Here, this was overcome in the proposed quadripartite photocatalyst, and no leached Cd(II) cations were observed at the end of the photodegradation process, as tested via spot test analysis of the solution against sulfide anions, and no yellow CdS was observed.

3.2.9 Effect of various waters

To test the applicability of the proposed quadripartite photocatalyst for photodegrading SFSZ in various water sources, SFSZ solutions were prepared in different water matrixes like distilled water, pool water (in our university), tap water (in our laboratory), well water (in our university), Zaiandehrood river (Isfahan, Iran), and Zarcheshmeh river (Semirom, Isfahan Iran) and the photodegradation experi-

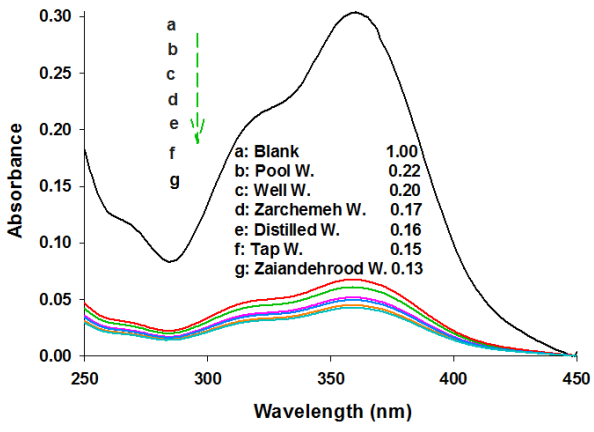

Figure 7. Effects of various waters on SFSZ removal by the proposed catalyst in the conditions of: catalysts dose 0.4 g/L, C_{SFSZ}: 6.25 mg/L, irradiation time: 30 min, pH 9.

ments were carried out under the RSM optimal runs' condition. The obtained UV-Vis spectra are compared in Fig. 7. As proved by the results, change in the water resource has no considerable effect on the activity of the photocatalyst, meaning that the photocatalyst can be excellently used in various wastewater samples for the successful photodegradation of SFSZ. As the results show, a relatively small change in the obtained C/Co values (inversely, as a measure of the photodegraded SFSZ molecules) was obtained with various water samples concerning the SFSZ solution prepared in distilled water. In these cases, some inorganic species may scavenge some reactive species and slightly decrease the degradation efficiency. In contrast, some inorganic substances may produce reactive radicals that can enhance photodegradation efficiency. It is worth mentioning that no analysis was done on the water samples used, and they were used to prepare SFSZ solutions as received.

4. Conclusions

A synergistic photocatalytic activity was achieved for the quadripartite catalyst, concerning the individual catalyst and their binary system. This boosted effect can be related to the efficient e/h separation in the quadripartite catalyst that is well described by the direct Z-scheme mechanism, consisting of 3 binary Z-scheme systems sequentially connected. In the first Z-scheme system (WO_3-$BiVO_4$), the potential positions of CB-WO_3 are negative enough to allow electron transfer to the VB-$BiVO_4$. In the second Z-scheme, electron transfers from the VB-$BiVO_4$ to the VB-CdS position. The third Z-scheme system forms between the CdS-Cu_2O, which finally accumulates the electrons in CB-Cu_2O. These CB-Cu_2O electrons are more powerful reducing centers than the CB- WO_3 accumulated electrons in the type II-heterojunction mechanism and can produce enough superoxide radicals. These electrons can also directly reduce SFSZ molecules (E: about 0.75 V). As proved by scavenging agents, superoxide radicals can also react with SFSZ molecules, which are the more effective species. In this direct Z-scheme mechanism, the holes must be accumulated in VB-WO_3 as more powerful oxidizing agents than those of VB-Cu_2O in the type II-heterojunction system. These accumulated holes can effectively oxidize water to hydroxyl radicals as the second critical center for SFSZ photodegradation based on the results obtained in the scavenging agent study. Based on the results, the successive direct Z-scheme system is suitable for illustrating the SFSZ photodegradation using the proposed quadripartite catalyst.

Acknowledgment
The authors thank Mohammad Alizadeh and Mohammad Hossein Kazemzadeh for performing instrumental analysis of the samples, as experts in laboratory analysis in Shahreza Branch, Islamic Azad University, Isfahan, Iran. The authors also thank the president of Shahreza Branch, Islamic Azad University, Iran, for supporting this work.

Authors contributions
Authors have contributed equally in preparing and writing the manuscript.

Availability of data and materials
The data that support the findings of this study are available from the corresponding author, upon reasonable request.

Conflict of interests
The author declare that they have no known competing financial interests or personal relationships that could have appeared to influence the work reported in this paper.

References

[1] M. S. Salman, M. C. Sheikh, M. M. Hasan, M. N. Hasan, K. T. Kubra, A. I. Rehan, M. E. Awual, A. I. Rasee, R. M. Waliullah, M. S. Hossain, M. A. Khaleque, A. K. D. Alsukaibi, H. M. Alshammari, and M. R. Awual. *Appl. Surf. Sci.*, **622**(2023):157008. DOI: https://doi.org/10.1016/j.apsusc.2023.157008.

[2] K. T. Kubra, M. M. Hasan, M. N. Hasan, M. S. Salman, M. A. Khaleque, M. C. Sheikh, A. I. Rehan, A. I. Rasee, R. M. Waliullah, M. E. Awual, M. S. Hossain, A. K. D. Alsukaibi, H. M. Alshammari, and M. R. Awual. *Colloids Surf. Physicochem. Eng. Aspects*, **667**(2023):131415, . DOI: https://doi.org/10.1016/j.colsurfa.2023.131415.

[3] K. T. Kubra, M. S. Salman, and M. N. Hasan. *J. Mol. Liq.*, **328**(2021):115468, . DOI: https://doi.org/10.1016/j.molliq.2021.115468.

[4] M. R. Awual, M. N. Hasan, M. M. Hasan, M. S. Salman, M. C. Sheikh, K. T. Kubra, M. S. Islam, H. M. Marwani, A. Islam, M. A. Khaleque, R. M. Waliullah, M. S. Hossain, A. I. Rasee, A. I. Rehan, and M. E. Awual. *Sep. Purif. Technol.*, **319**(2023):124088, . DOI: https://doi.org/10.1016/j.seppur.2023.124088.

[5] M. R. Awual. *Chem. Eng. J.*, **307**(2017):456–465. DOI: https://doi.org/10.1016/j.cej.2016.08.108.

[6] M. R. Awual, M. M. Hasan, G. E. Eldesoky, M. A. Khaleque, M. M. Rahman, and M. Naushad. *Chem. Eng. J.*, **290**(2016):243–251, . DOI: https://doi.org/10.1016/j.cej.2016.01.038.

[7] M. Zheng, J. Chen, L. Zhang, Y. Cheng, C. Lu, Y. Liu, A. Singh, M. Trivedi, A. Kumar, and J. Liu. *Mater. Today Commun.*, **31**(2022): 103514. DOI: https://doi.org/10.1016/j.mtcomm.2022.103514.

[8] J. Wang, C. Rao, L. Lu, S. Zhang, M. Muddassir, and J. Liu. *CrystEngComm*, **23**(2021):741–747. DOI: https://doi.org/10.1039/D0CE01632B.

[9] Y. Wu, X. He, X. Wang, J. Xv, M. Muddassir, I. A. Ansari, and A. Zhong. *Inorg. Chim. Acta*, **568**(2024):122115. DOI: https://doi.org/10.1016/j.ica.2024.122115.

[10] X. Dong, Y. Li, D. Li, D. Liao, T. Qin, O. Prakash, A. Kumar, and J. Liu. *CrystEngComm*, **24**(2022):6933–6943. DOI: https://doi.org/10.1039/D2CE01121B.

[11] R. Xiang, C. Zhou, Y. Liu, T. Qin, D. Li, X. Dong, M. Muddassir, and A. Zhong. *J. Mol. Struct.*, **1312**(2024):138501. DOI: https://doi.org/10.1016/j.molstruc.2024.138501.

[12] N. Pugazhenthiran, S. Murugesan, P. Sathishkumar, and S. Anandan. *Chem. Eng. J.*, **241**(2014):401–409. DOI: https://doi.org/10.1016/j.cej.2013.10.069.

[13] Y. Ji, Y. Yang, L. Zhou, L. Wang, J. Lu, C. Ferronato, and J. M. Chovelon. *Water Res.*, **133**(2018):299–309. DOI: https://doi.org/10.1016/j.watres.2018.01.047.

[14] C. F. Carolin, P. S. Kumar, A. Saravanan, G. J. Joshiba, and M. Naushad. *J. Environ. Chem. Eng.*, **5**(2017):2782–2799. DOI: https://doi.org/10.1016/j.jece.2017.05.029.

[15] M. R. Awual, M. M. Hasan, J. Iqbal, M. A. Islam, A. Islam, S. Khandaker, A. M. Asiri, and M. M. Rahman. *J. Environ. Chem. Eng.*, **8**(2020):103591, . DOI: https://doi.org/10.1016/j.jece.2019.103591.

[16] M. R. Awual, M. M. Hasan, A. M. Asiri, and M. M. Rahman. *Compos. B Eng.*, **171**(2019):294–301, . DOI: https://doi.org/10.1016/j.compositesb.2019.05.078.

[17] K. T. Kubra, M. S. Salman, H. Znad, and M. N. Hasan. *J. Mol. Liq.*, **329**(2021):115541, . DOI: https://doi.org/10.1016/j.molliq.2021.115541.

[18] R. M. Waliullah, A. I. Rehan, M. E. Awual, A. I. Rasee, M. C. Sheikh, M. S. Salman, M. S. Hossain, M. M. Hasan, K. T. Kubra, M. N. Hasan, H. M. Marwani, A. Islam, M. M. Rahman, M. A. Khaleque, and M. R. Awual. *J. Mol. Liq.*, **388**(2023):122763. DOI: https://doi.org/10.1016/j.molliq.2023.122763.

[19] T. D. Pham, T. T. Bui, T. T. Trang Truong, T. H. Hoang, T. S. Le, V. D. Duong, A. Yamaguchi, M. Kobayashi, and Y. Adachi. *J. Mol. Liq.*, **298**(2020):111981. DOI: https://doi.org/10.1016/j.molliq.2019.111981.

[20] I. Luhar, S. Luhar, M. M. A. B. Abdullah, R. A. Razak, P. Vizureanu, A. V. Sandu, and P. D. Matasaru. *Materials*, **14**(2021):7456. DOI: https://doi.org/10.3390/ma14237456.

[21] A. Rafiq, M. Ikram, S. Ali, F. Niaz, M. Khan, Q. Khan, and M. Maqbool. *J. Indust. Eng. Chem.*, **97**(2021):111–128. DOI: https://doi.org/10.1016/j.jiec.2021.02.017.

[22] V. Soni, A. Khosla, P. Singh, V. H. Nguyen, Q. V. Le, R. Selvasembian, C. M. Hussain, S. Thakur, and P. Raizada. *J. Environ. Manage.*, **308**(2022):114617. DOI: https://doi.org/10.1016/j.jenvman.2022.114617.

[23] M. Malhotra, A. Sudhaik, Sonu, P. Raizada, T. Ahamad, V. H. Nguyen, Q. Van Le, R. Selvasembian, A. K. Mishra, and P. Singh. *Ind. Crop. Prod.*, **202**(2023):117000, . DOI: https://doi.org/10.1016/j.indcrop.2023.117000.

[24] A. Ajmal, I. Majeed, R. N. Malik, M. Iqbal, M. A. Nadeem, I. Hussain, S. Yousaf, Zeshan, G. Mustafa, M. I. Zafar, and M. A. Nadeem. *J. Environ. Chem. Eng.*, **4**(2016):2138–2146. DOI: https://doi.org/10.1016/j.jece.2016.03.041.

[25] J. Rezaee, F. Salimi, and C. Karami. *Desalination and Water Treatment*, **139**(2019):342–351. DOI: https://doi.org/10.5004/dwt.2019.23270.

[26] I. Hasan and F. A. Alharthi. *J. Photochem. Photobiol. A: Chem*, **433**(2022):114126. DOI: https://doi.org/10.1016/j.jphotochem.2022.114126.

[27] C. Rao, L. Zhou, Y. Pan, C. Lu, X. Qin, H. Sakiyama, M. Muddassir, and J. Liu. *J. Alloys Compd.*, **897**(2022):163178. DOI: https://doi.org/10.1016/j.jallcom.2021.163178.

[28] A. Kumar, P. Singh, A. A. P. Khan, Q. V. Le, V. H. Nguyen, S. Thakur, and P. Raizada. *Chem. Eng. J.*, **439**(2022):135563, . DOI: https://doi.org/10.1016/j.cej.2022.135563.

[29] P. L. Meena, A. K. Surela, L. K. Chhachhia, J. Meena, and R. Meena. *Nan. Adv.*, (2025), . DOI: https://doi.org/10.1039/D4NA00890A.

[30] P. L. Meena, K. Poswal, A. K. Surela, and J. K. Saini. *Adv. Compos. Hybrid Mater.*, **6**(2022):16, . DOI: https://doi.org/10.1007/s42114-022-00577-1.

[31] P. L. Meena, K. Poswal, A. K. Surela, K. S. Meena, and B. Mordhiya. *Environ. Sci. Pollut. Res.*, **30**(2023):68770–68791, . DOI: https://doi.org/10.1007/s11356-023-27215-7.

[32] P. L. Meena, L. K. Chhachhia, and A. K. Surela. *J. Mol. Struct.*, **1303**(2024):137575, . DOI: https://doi.org/10.1016/j.molstruc.2024.137575.

[33] W. Nam, K. Woo, and G. Han. *J. Indust. Eng. Chem.*, **15**(2009): 348–353. DOI: https://doi.org/10.1016/j.jiec.2008.11.006.

[34] Z. Ciğeroğlu, S. Şahin, and E. S. Kazan. *Biomass Convers. Biorefin.*, **12**(2022):73–86. DOI: https://doi.org/10.1007/s13399-021-01734-0.

[35] Z. Esmaili, A. R. Solaimany Nazar, and M. Farhadian. *Sci. Iranica*, **24**(2017):1221–1229. DOI: https://doi.org/10.24200/sci.2017.4106.

[36] D. Ye, L. Liu, Q. Peng, J. Qiu, H. Gong, A. Zhong, and S. Liu. *Molecules*, (2023). DOI: https://doi.org/10.3390/molecules28114507.

[37] M. S. AlSalhi, A. Sakthisabarimoorthi, S. Devanesan, S. A. Martin Britto Dhas, and M. Jose. *J. Mater. Sci.: Mater. Electron.*, **30**(2019):13708–13718. DOI: https://doi.org/10.1007/s10854-019-01752-9.

[38] C. EL Bekkali, H. Bouyarmane, S. Laasri, A. Laghzizil, and A. Saoiabi. *Iran. J. Catal.*, **8**(2018):241–247.

[39] P. L. Meena, L. K. Chhachhia, and A. K. Surela. *Opt. Mater.*, **148**(2024):114916, . DOI: https://doi.org/10.1016/j.optmat.2024.114916.

[40] N. Ahmad, J. Anae, M. Z. Khan, S. Sabir, X. J. Yang, V. K. Thakur, P. Campo, and F. Coulon. *J. Environ. Manage.*, **295**(2021):113362. DOI: https://doi.org/10.1016/j.jenvman.2021.113362.

[41] W. L. da Silva, D. M. Druzian, L. R. Oviedo, P. C. L. Muraro, and V. R. Oviedo. *Silver Nanoparticles for Photocatalysis and Biomedical Applications, Silver Micro-Nanoparticles-Properties, Synthesis, Characterization, and Applications, IntechOpen2021*, **256**(2012):1479–1508.

[42] A. Eslami, A. Oghazyan, and M. Sarafraz. *Iran. J. Catal.*, **8**(2018): 95–102.

[43] M. Zebardast, A. Fallah Shojaei, and K. Tabatabaeian. *Iran. J. Catal.*, **8**(2018):297–309.

[44] M. V. Kangralkar and M. Jayappa. *Iran. J. Catal.*, **10**(2020):181–188.

[45] M. Yaghoubi-berijani, B. Bahramian, and S. Zargari. *Iran. J. Catal.*, **10**(2020):307–317.

[46] A. Karami, R. Monsef, I. Waleed, H. L. Kareem, I. T. Ibrahim, and M. Salavati-Niasari. *Int. J. Hydrogen Energy*, **48**(2023):8499–8513. DOI: https://doi.org/10.1016/j.ijhydene.2022.12.017.

[47] A. Panahi, R. Monsef, S. A. Hussein, S. A. Hammood, W. K. Al-Azzawi, D. E. Raffik, F. S. Hashim, and M. Salavati-Niasari. *Int. J. Hydrogen Energy*, **48**(2023):33155–33165. DOI: https://doi.org/10.1016/j.ijhydene.2023.05.125.

[48] P. L. Meena, K. Poswal, A. K. Surela, and J. K. Saini. *Int. J. Environ. Sci. Technol. (Tehran)*, (2024), . DOI: https://doi.org/10.1007/s13762-024-05704-7.

[49] H. Nguyen Phuoc, Q. T. Le, T. C. T. Pham, and T. T. Le. *ACS Omega*, **6**(2021):21024–21032. DOI: https://doi.org/10.1021/acsomega.1c02658.

[50] H. Tehubijuluw, R. Subagyo, Y. Kusumawati, and D. Prasetyoko. *Sustain. Environ. Res.*, **32**(2022):4. DOI: https://doi.org/10.1186/s42834-021-00113-8.

[51] R. O. A. Rahman, A. M. El-Kamash, and Y. T. Hung. *Water*, **14**(2022):137.
DOI: https://doi.org/10.3390/w14020137.

[52] A. Singh, A. K. Singh, J. Liu, and A. Kumar. *Catal. Sci. Technol.*, **11**(2021):3946–3989.
DOI: https://doi.org/10.1039/D0CY02275F.

[53] J. Piriyanon, T. Chankhanittha, S. Youngme, K. Hemavibool, S. Nijpanich, S. Juabrum, N. Chanlek, and S. Nanan. *J. Mater. Sci.: Mater. Electron.*, **32**(2021):19798–19819.
DOI: https://doi.org/10.1007/s10854-021-06504-2.

[54] N. AttariKhasraghi, K. Zare, A. Mehrizad, N. Modirshahla, and M. A. Behnajady. *J. Inorg. Organomet. Polym. Mater.*, **31**(2021):3164–3174.
DOI: https://doi.org/10.1007/s10904-021-01967-6.

[55] A. Gulino, G. Papanikolaou, P. Lanzafame, A. Aaliti, P. Primerano, L. Spitaleri, C. Triolo, Z. Dahrouch, A. Khaskhoussi, and S. Lo Schiavo. *ChemistryOpen*, **10**(2021):1033–1040.
DOI: https://doi.org/10.1002/open.202100157.

[56] D. Adenuga, S. Skosana, S. Tichapondwa, and E. Chirwa. *RSC Adv.*, **11**(2021):36760–36768.
DOI: https://doi.org/10.1039/D1RA06855E.

[57] K. Sun, G. Zhan, H. Chen, and S. Lin. *Sensors*, **21**(2021):8269.
DOI: https://doi.org/10.3390/s21248269.

[58] K. Sharma, A. Sudhaik, P. Raizada, P. Thakur, X. M. Pham, Q. Van Le, V. H. Nguyen, T. Ahamad, S. Thakur, and P. Singh. *Environ. Sci. Pollut. Res.*, **30**(2023):124902–124920, .
DOI: https://doi.org/10.1007/s11356-022-24940-3.

[59] N. Kumar, M. Kumari, M. Ismael, M. Tahir, R. K. Sharma, K. Kumari, J. R. Koduru, and P. Singh. *Environ. Res.*, **231**(2023):116149, .
DOI: https://doi.org/10.1016/j.envres.2023.116149.

[60] P. Dhull, A. Sudhaik, V. Sharma, P. Raizada, V. Hasija, N. Gupta, T. Ahamad, V. H. Nguyen, A. Kim, M. Shokouhimehr, S. Y. Kim, Q. V. Le, and P. Singh. *Mol. Catal.*, **539**(2023):113013.
DOI: https://doi.org/10.1016/j.mcat.2023.113013.

[61] A. Rostami-Vartooni, A. Moradi-Saadatmand, M. Bagherzadeh, and M. Mahdavi. *Iran. J. Catal.*, **9**(2019):27–35.

[62] A. Sobhani-Nasab, M. Eghbali-Arani, S. M. Hosseinpour-Mashkani, F. Ahmadi, M. Rahimi-Nasrabadi, and V. Ameri. *Iran. J. Catal.*, **10**(2020):91–99.

[63] M. Samandari, A. Taghva Manesh, S. A. Hosseini, and S. Mansouri. *Iran. J. Catal.*, **11**(2021):175–180.

[64] P. L. Meena, K. Poswal, A. K. Surela, and J. K. Saini. *Water Sci. Technol.*, **84**(2021):2615–2634, .
DOI: https://doi.org/10.2166/wst.2021.431.

[65] F. S. Alamro, A. M. Mostafa, K. A. Abu Al-Ola, H. A. Ahmed, and A. Toghan. *Nanomaterials*, **11**(2021):2142.
DOI: https://doi.org/10.3390/nano11082142.

[66] A. A. Manda, K. A. Elsayed, U. I. Gaya, S. A. Haladu, I. Ercan, F. Ercan, M. Alheshibri, A. Al Baroot, T. S. Kayed, S. Alshammery, N. A. Altamimi, and A. L. Al-Otaibi. *Optics & Laser Technology*, **155**(2022):108430.
DOI: https://doi.org/10.1016/j.optlastec.2022.108430.

[67] K. A. Isai and V. S. Shrivatava. *Iran. J. Catal.*, **9**(2019):259–268.

[68] A. Islam, S. H. Teo, M. T. Islam, A. H. Mondal, H. Mahmud, S. Ahmed, M. Ibrahim, Y. H. Taufiq-Yap, A. A. G, M. L. Hossain, M. C. Sheikh, A. I. Rasee, A. I. Rehan, R. M. Waliullah, M. E. Awual, M. M. Hasan, M. S. Hossain, K. T. Kubra, M. S. Salman, M. N. Hasan, and M. R. Awual. *Renew. Sustain. Energy Rev.*, **208**(2025):115033.
DOI: https://doi.org/10.1016/j.rser.2024.115033.

[69] K. Sharma, A. Kumar, T. Ahamad, Q. V. Le, P. Raizada, A. Singh, L. H. Nguyen, S. Thakur, V. H. Nguyen, and P. Singh. *Journal of Materials Science & Technology*, **152**(2023):50–64, .
DOI: https://doi.org/10.1016/j.jmst.2022.11.053.

[70] K. Sharma, S. Sonu, A. Sudhaik, T. Ahamad, S. Kaya, S. Thakur, Q. V. Le, V. H. Nguyen, A. Singh, L. H. Nguyen, P. Singh, and P. Raizada. *J. Water Proc. Eng.*, **66**(2024):105918, .
DOI: https://doi.org/10.1016/j.jwpe.2024.105918.

[71] V. Hasija, A. A. Parwaz Khan, Sonu, K. P. Katin, S. Kaya, P. Singh, P. Raizada, M. Asad, M. A. Rub, and K. A. Alzahrani. *Solid State Sci.*, **157**(2024):107693.
DOI: https://doi.org/10.1016/j.solidstatesciences.2024.107693.

[72] A. Rana, Sonu, A. Sudhaik, A. Chawla, P. Raizada, A. K. Kaushik, T. Ahamad, S. Kaya, N. Kumar, and P. Singh. *Indust. Eng. Chem. Res.*, **63**(2024):6960–6973.
DOI: https://doi.org/10.1021/acs.iecr.4c00101.

[73] J. P. Chang, C. Y. Wang, Y. J. Hsu, and C. Y. Wang. *Appl. Catal., A*, **650**(2023):119005.
DOI: https://doi.org/10.1016/j.apcata.2022.119005.

[74] S. Obregón, A. Caballero, and G. Colón. *Applied Catalysis B: Environmental*, **117-118**(2012):59–66.
DOI: https://doi.org/10.1016/j.apcatb.2011.12.037.

[75] H. F. Lai, C. C. Chen, Y. K. Chang, C. S. Lu, and R. J. Wu. *Sep. Purif. Technol.*, **122**(2014):78–86.
DOI: https://doi.org/10.1016/j.seppur.2013.10.049.

[76] S. S. Dunkle, R. J. Helmich, and K. S. Suslick. *J. Physic. Chem. C.*, **113**(2009):11980–11983.
DOI: https://doi.org/10.1021/jp903757x.

[77] E. Aguilera-Ruiz, U. M. García-Pérez, M. de la Garza-Galván, P. Zambrano-Robledo, B. Bermúdez-Reyes, and J. Peral. *Appl. Surf. Sci.*, **328**(2015):361–367.
DOI: https://doi.org/10.1016/j.apsusc.2014.12.059.

[78] S. Selvarajan, A. Suganthi, M. Rajarajan, and K. Arunprasath. *Powder Technol*, **307**(2017):203–212.
DOI: https://doi.org/10.1016/j.powtec.2016.10.069.

[79] N. Omrani and A. Nezamzadeh-Ejhieh. *J. Photochem. Photobiol. A: Chem.*, **400**(2020):112726, .
DOI: https://doi.org/10.1016/j.jphotochem.2020.112726.

[80] S. Arshadi-Rastabi, J. Moghaddam, and M. Reza Eskandarian. *J. Indust. Eng. Chem.*, **22**(2015):34–40.
DOI: https://doi.org/10.1016/j.jiec.2014.06.022.

[81] N. Qutub, B. M. Pirzada, K. Umar, and S. Sabir. *J. Environ. Chem. Eng.*, **4**(2016):808–817.
DOI: https://doi.org/10.1016/j.jece.2015.10.031.

[82] A. Martínez de la Cruz and U. M. G. Pérez. *Mater. Res. Bull.*, **45**(2010):135–141.
DOI: https://doi.org/10.1016/j.materresbull.2009.09.029.

[83] N. Omrani and A. Nezamzadeh-Ejhieh. *J. Mol. Liq.*, **315**(2020):113701, .
DOI: https://doi.org/10.1016/j.molliq.2020.113701.

[84] N. Omrani and A. Nezamzadeh-Ejhieh. *Environ. Sci. Pollut. Res.*, **27**(2020):44292–44305, .
DOI: https://doi.org/10.1007/s11356-020-10278-1.

[85] N. Omrani and A. Nezamzadeh-Ejhieh. *Int. J. Hydrogen Energy*, **45**(2020):19144–19162, .
DOI: https://doi.org/10.1016/j.ijhydene.2020.05.019.

[86] N. Omrani and A. Nezamzadeh-Ejhieh. *J. Water Proc. Engineering*, **33**(2020):101094, .
DOI: https://doi.org/10.1016/j.jwpe.2019.101094.

[87] N. Omrani and A. Nezamzadeh-Ejhieh. *Sep. Purif. Technol.*, **235**(2020):116228, .
DOI: https://doi.org/10.1016/j.seppur.2019.116228.

[88] N. Omrani, A. Nezamzadeh-Ejhieh, and M. Alizadeh. *Desal. Water Treat*, **162**(2019):290–304.
DOI: https://doi.org/10.5004/dwt.2019.24352.

[89] P. Rodríguez, N. Muñoz-Aguirre, E. S. M. Martínez, G. Gonzalez, O. Zelaya, and J. Mendoza. *Appl. Surf. Sci.*, **255**(2008):740–742.
DOI: https://doi.org/10.1016/j.apsusc.2008.07.032.

[90] M. Amiri, A. Pardakhti, M. Ahmadi-Zeidabadi, A. Akbari, and M. Salavati-Niasari. *Colloids Surf. B. Biointerfaces*, **172**(2018):244–253.
DOI: https://doi.org/10.1016/j.colsurfb.2018.08.049.

[91] M. El Bouraie and S. Ibrahim. *Int. J. Nanomed.*, **15**(2020):7117.
DOI: https://doi.org/10.2147/IJN.S265739.

[92] T. Seyedi-Chokanlou, S. Aghabeygi, N. Molahasani, and F. Abrinaei. *Iran. J. Catal.*, **11**(2021):49–58.

[93] B. Manikandan, K. Murali, and R. John. *Iran. J. Catal.*, **11**(2021):1–11.

[94] M. Arunkumar and A. Samson Nesaraj. *Iran. J. Catal.*, **10**(2020):235–245.

[95] R. J. Manikandan Balakrishnan. *Iran. J. Catal.*, **10**(2020):1–16.

[96] M. Salavati-Niasari, P. Salemi, and F. Davar. *J. Mol. Catal. A: Chem.*, **238**(2005):215–222.
DOI: https://doi.org/10.1016/j.molcata.2005.05.026.

[97] F. Mazloom, M. Masjedi-Arani, M. Ghiyasiyan-Arani, and M. Salavati-Niasari. *J. Mol. Liq.*, **214**(2016):46–53.
DOI: https://doi.org/10.1016/j.molliq.2015.11.033.

[98] S. Landi, I. R. Segundo, E. Freitas, M. Vasilevskiy, J. Carneiro, and C. J. Tavares. *Solid State Commun.*, **341**(2022):114573.
DOI: https://doi.org/10.1016/j.ssc.2021.114573.

[99] S. K. Suram, P. F. Newhouse, and J. M. Gregoire. *ACS Comb. Sci.*, **18**(2016):673–681.
DOI: https://doi.org/10.1021/acscombsci.6b00053.

[100] M. Shaterian, M. Enhessari, D. Rabbani, M. Asghari, and M. Salavati-Niasari. *Appl. Surf. Sci.*, **318**(2014):213–217.
DOI: https://doi.org/10.1016/j.apsusc.2014.03.087.

[101] P. Norouzzadeh, K. Mabhouti, M. Golzan, and R. Naderali. *Optik*, **204**(2020):164227.
DOI: https://doi.org/10.1016/j.ijleo.2020.164227.

[102] P. Makuła, M. Pacia, and W. Macyk. *J. Phys. Chem. Lett.*, **9**(2018):6814–6817, .
DOI: https://doi.org/10.1021/acs.jpclett.8b02892.

[103] J. Tauc. *North-Holland Publishing Company, Amsterdam*, (1972).

[104] J. B. Coulter and D. P. Birnie III. *Phys. Status Solidi (B)*, **255**(2018):1700393, .
DOI: https://doi.org/10.1002/pssb.201700393.

[105] R. Köferstein, L. Jäger, and S. G. Ebbinghaus. *Solid State Ionics*, **249-250**(2013):1–5.
DOI: https://doi.org/10.1016/j.ssi.2013.07.001.

[106] R. Köferstein and S. G. Ebbinghaus. *J. Eur. Ceram. Soc.*, **37**(2017):1509–1516.
DOI: https://doi.org/10.1016/j.jeurceramsoc.2016.12.014.

[107] K. i. Katsumata, R. Motoyoshi, N. Matsushita, and K. Okada. *J. Hazard. Mater.*, **260**(2013):475–482.
DOI: https://doi.org/10.1016/j.jhazmat.2013.05.058.

[108] P. Makuła, M. Pacia, and W. Macyk. *J. Phys. Chem. Lett.*, **9**(2018):6814–6817, .
DOI: https://doi.org/10.1021/acs.jpclett.8b02892.

[109] J. B. Coulter and D. P. Birnie III. *Phys. Status Solidi B*, **255**(2018):1700393, .
DOI: https://doi.org/10.1002/pssb.201700393.

[110] H. Che, G. Che, E. Jiang, C. Liu, H. Dong, and C. Li. *J. Taiwan Inst. Chem. Eng.*, **91**(2018):224–234.

[111] S. Dianat. *Iran. J. Catal.*, **8**(2018):121–132.

[112] S. Muhammad, S. T. Hussain, M. Waseem, A. Naeem, J. Hussain, and M. Tariq Jan. *Iranian J. Sci. and Technol. (Sciences)*, **36**(2012):481–486.
DOI: https://doi.org/10.22099/ijsts.2012.2110.

[113] M. M. Emara, S. H. Ali, A. A. Hassan, T. S. E. Kassem, and P. G. Van Patten. *Colloid and Inter. Sci. Commun.*, **40**(2021):100341.
DOI: https://doi.org/10.1016/j.colcom.2020.100341.

[114] C. W. Tsao, M. J. Fang, and Y. J. Hsu. *Coord. Chem. Rev.*, **438**(2021):213876.
DOI: https://doi.org/10.1016/j.ccr.2021.213876.

[115] S. Yousefzadeh, A. R. Matin, E. Ahmadi, Z. Sabeti, M. Alimohammadi, H. Aslani, and R. Nabizadeh. *Food Chem. Toxicol.*, **114**(2018):334–345.
DOI: https://doi.org/10.1016/j.fct.2018.02.045.

[116] N. Najafian, A. Aarabi, and A. Nezamzadeh-Ejhieh. *Iranian J. of Chem. and Chem. Eng.*, **42**(2023):601–617.
DOI: https://doi.org/10.30492/ijcce.2022.541486.4992.

[117] A. H. Khangah, M. J. Sarraf, H. Ale Ebrahim, and M. Tabatabaee. *Iran. J. Catal.*, **10**(2020):135–148.

[118] H. Salavati, A. Teimouri, and S. Kazemi. *Iran. J. Catal.*, **7**(2017):303–315.

[119] M. Massoudinejad, M. Sadani, Z. Gholami, Z. Rahmati, M. Javaheri, H. Keramati, M. Sarafraz, M. Avazpour, and S. Shiri. *Iran. J. Catal.*, **9**(2019):121–132.

[120] N. Parsafard. *Iran. J. Catal.*, **13**(2023):125–133.

[121] K. Govindan, H. T. Chandran, M. Raja, S. U. Maheswari, and M. Rangarajan. *J. Photochem. Photobiol. A: Chem.*, **341**(2017):146–156.
DOI: https://doi.org/10.1016/j.jphotochem.2017.03.025.

[122] D. Vione, S. Khanra, S. C. Man, P. R. Maddigapu, R. Das, C. Arsene, R. I. Olariu, V. Maurino, and C. Minero. *Water Res.*, **43**(2009):4718–4728.
DOI: https://doi.org/10.1016/j.watres.2009.07.032.

[123] T. Tan, D. Beydoun, and R. Amal. *J. Photochem. Photobiol. A: Chem.*, **159**(2003):273–280.
DOI: https://doi.org/10.1016/S1010-6030(03)00171-0.

[124] H. Sapper, S. O. Kang, H. H. Paul, and W. Lohmann. *Z Naturforsch C Biosci*, **37**(1982):942–946.

[125] A. Nandi and I. B. Chatterjee. *J. Biosci. (Bangalore)*, **11**(1987):435–441.
DOI: https://doi.org/10.1007/BF02704692.

[126] Q. Xu, L. Zhang, J. Yu, S. Wageh, A. A. Al-Ghamdi, and M. Jaroniec. *Mater. Today*, **21**(2018):1042–1063.
DOI: https://doi.org/10.1016/j.mattod.2018.04.008.

[127] Y. C. Pu, W. H. Lin, and Y. J. Hsu. *Appl. Catal. B.*, **163**(2015):343–351.
DOI: https://doi.org/10.1016/j.apcatb.2014.08.009.

[128] J. M. Li, C. W. Tsao, M. J. Fang, C. C. Chen, C. W. Liu, and Y. J. Hsu. *ACS Appl. Nano Mater.*, **1**(2018):6843–6853.
DOI: https://doi.org/10.1021/acsanm.8b01678.

[129] R. M. Buoro, V. C. Diculescu, I. C. Lopes, S. H. P. Serrano, and A. M. Oliveira-Brett. *Electroanalysis*, **26**(2014):924–930. DOI: https://doi.org/10.1002/elan.201400053.

[130] V. Dutta, S. Sonu, P. Raizada, V. K. Thakur, T. Ahamad, S. Thakur, P. Kumar Verma, H. H. P. Quang, V. H. Nguyen, and P. Singh. *Environ. Sci. Pollut. Res. Int.*, **30**(2023):124530–124545. DOI: https://doi.org/10.1007/s11356-022-20743-8.

[131] K. Sharma, V. Hasija, M. Malhotra, P. K. Verma, A. A. Parwaz Khan, S. Thakur, Q. Van Le, H. H. Phan Quang, V. H. Nguyen, P. Singh, and P. Raizada. *Int. J. Hydrogen Energy*, **52**(2024):804–818, . DOI: https://doi.org/10.1016/j.ijhydene.2023.09.033.

[132] Y. Kumar, A. Sudhaik, K. Sharma, Sonu, P. Raizada, A. Aslam Parwaz Khan, V. H. Nguyen, T. Ahamad, P. Singh, and A. M. Asiri. *J. Photochem. Photobiol. A: Chem.*, **435**(2023):114326, . DOI: https://doi.org/10.1016/j.jphotochem.2022.114326.

[133] M. Malhotra, K. Poonia, P. Singh, A. A. P. Khan, P. Thakur, Q. Van Le, E. T. Helmy, T. Ahamad, V. H. Nguyen, S. Thakur, and P. Raizada. *J. Taiwan Inst. Chem. Eng.*, **158**(2024):104945, . DOI: https://doi.org/10.1016/j.jtice.2023.104945.

[134] A. A. Parwaz Khan, P. Singh, P. Raizada, A. Khan, A. M. Asiri, and M. M. Alotaibi. *Chemosphere*, **316**(2023):137839. DOI: https://doi.org/10.1016/j.chemosphere.2023.137839.

[135] A. Kumar, P. Singh, V. H. Nguyen, Q. Van Le, T. Ahamad, S. Thakur, L. Huong Nguyen, and P. Raizada. *Chem. Eng. J.*, **474**(2023):145720, . DOI: https://doi.org/10.1016/j.cej.2023.145720.